Interference-Based Micromechanical Spectral Equalizers

J. E. Ford, K. W. Goossen, J. A. Walker, D. T. Neilson, D. M. Tennant, S. Y. Park, J. W. Sulhoff

Abstract— **Dynamic gain equalization filters (DGEF) are important for high-performance WDM communications. One of the first demonstrated DGEF used a micromechanical etalon filter array illuminated with free-space spectral demultiplexing optics. Here we present subsequent research on etalon-based dynamic spectral filters, including vertical device structures which linearize and reduce the drive voltage from 70 to 40V, and spatially-segmented etalons which allow channelized spectral equalization and further reduce drive voltage. We describe a prototype using a simplified cylindrical opto-mechanical package with a 104 nm broadband spectral response, 7.5 dB insertion loss and less than 16V operation voltage. Finally, we show the use of a 42 nm bandwidth DGEF prototype and feedback stabilization to more than double the number of channels and operating bandwidth of a conventional Erbium-doped fiber amplifier (EDFA) while maintaining <1 dB power uniformity.**

Index Terms— **dynamic gain equalizing filters, MEMS components, micro-electro-mechanical systems, amplifiers.**

I. Introduction

ACTIVE POWER level stabilization is of great importance for high capacity wavelength division multiplexed (WDM) transmission systems. The initial requirement was for dynamic gain equalization filters (DGEF) [1], which produce a smoothly varying spectral attenuation profile to remove variations in channel net gain profiles. The spectral resolution required corresponds to the amplifier gain variances, which are many wavelength channels wide (typically 0.8 to 1.6 nm each). A range of attenuation of 20 dB or more is typically needed, although specific applications can vary. The various solutions proposed and demonstrated for this application include micro-mechanical based systems [2,3], liquid-crystal [4-7], acousto-optic [8], and waveguide [9] technologies. A second generation of spectral equalizers with greater spectral resolution was demanded in response to dynamic network reconfiguration, wherein individual wavelength channels can be switched in and out of a WDM transmission switches such as photonic cross connects and wavelength add/drop switches. Such transparent optical networking demands power level equalization of channels that have not only traversed components with non-uniform loss or gain, but may have arrived from diverse paths. Several technologies have been proposed for high resolution and dynamic range channelized equalizing filters including MEMS tilt-mirror arrays [10, 11], liquid crystal [5, 6] and planar light wave circuits [12].

Manuscript received October 16, 2003

J. E. Ford is with the University of California San Diego, Department of Electrical and Computer Engineering, 9500 Gilman Drive, La Jolla CA, 92093-0407, jeford@ucsd.edu; K. W. Goossen is with the University of Delaware; J.A.Walker is with JayWalker Technical Consulting; S. Y. Park is with OptoVia Corporation; D. M. Tennant and D. T. Neilson are with Bell Labs, Lucent Technologies, where this research was performed.

We previously demonstrated spectral equalization using free-space optics to disperse an input spectrum over a micro-opto-mechanical variable reflectivity etalon mirror [2]. The basic device structure, shown in Fig. 1, is a single-cavity etalon stripe with an electrically controlled gap between a silicon substrate and a silicon nitride λ/4 layer. Each pair of electrodes applies a local force to reduce the etalon gap from 1.1 to 0.9 μm and create smoothly varying changes in the mirror reflectivity along the length of an approximately 80 by 1500 μm optical window. Mechanical connection between adjacent regions of the membrane ensures a smoothly varying reflectivity profile.

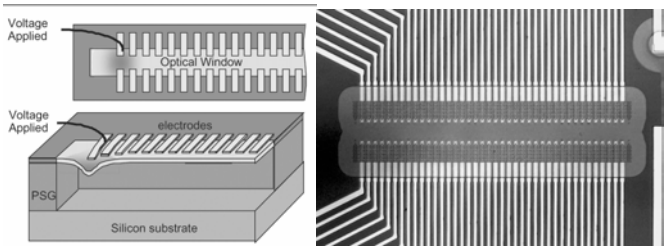

Figure 1: MEMS Micro-etalon structure (left) and fabricated device (right).

In this paper, we present subsequent research on etalon-based dynamic spectral filters, including materials and device structures which allow linearized and reduced voltage response, spatially-segmented etalons which allow channelized spectral equalization, a simplified and ruggedized opto-mechanical package. Finally, we demonstrate the use of the MEMS dynamic spectral equalizer to upgrade a conventional Erbium-doped fiber amplifier (EDFA) for increased numbers of WDM channels with wider operating parameters.

II. Optical System and Opto-Mechanical Package Design

The optomechanical package described in reference [2] used a skew optical path with vertical separation of the collimated input and output beams in the pupil to separate output signals. This package was functional, with some 4.6 dB insertion loss and < 0.2 dB polarization dependence, but optimization required 17 separate alignments: tip, tilt, z-shift and rotation of the grating, tip, tilt (two controls each) and focus of two collimators, x, y, z, tip and tilt of the MEMS device, focus of the imaging lens, and rotation of the quarterwave plate). As such this package was practical only as a laboratory testbed. The new optical design shown in Figure 2 considerably simplifies optical alignment. It consists of a coaxial imaging system with a diffraction grating at the collimated beam plane and an input/output fiber located in an

image plane adjacent to the MEMS device. Input and output signals are separated using an external optical circulator.

The optical demultiplexing system, illustrated in the raytrace of Figure 2, is constructed as a folded telecentric 4*f* system imaging system [13, 14]. The system consists of a *f* = 50 mm relay lens, with a planar 600 lp/mm grating in Littrow configuration (θ = 28.3°) at the stop. The lens is a full custom 4-element achromat designed for diffraction limited resolution over a 300 nm bandwidth, as compared to the 40 nm bandwidth of the original triplet lens [3]. Light enters an input fiber and passes through an optical circulator (not shown) then is emitted from the optical fiber into free space and imaged through the diffraction grating and two passes through the lens to arrive at the MEMS device spatially dispersed by wavelength. The MEMS membrane mirror reflects the light to retrace its path through the lens and grating and be re-multiplexed onto the face of the input fiber. Light coupled into the fiber propagates back to the circulator, which directs it into a separate output fiber.

This system is attractive because the full system path is 8f, i.e., two sequential relay imaging stages. If the MEMS device window is slightly oversized relative to the 10 μm optical mode diameter, then slight lateral misalignments of the system will be compensated on the second pass and returning light will automatically realign to the fiber core. Also, since the same lens and grating is used on both passes, the multiplexing and demultiplexing angles are automatically matched. This considerably relaxes alignment and focal length tolerances.

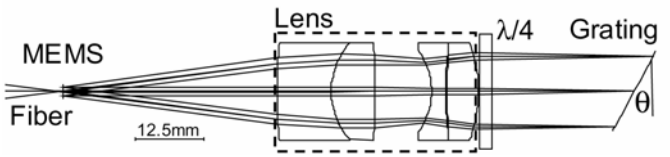

Figure 2 Optical layout for equalizing filter, including custom double-Gauss achromatic collimation / focus lens. Distance from grating to image is 100mm. (optical circulator used to separate input and output not shown).

Figure 3: Free-space WDM optomechanics, showing header, 50mm focal length lens and 600 lp/mm grating. At right, a close-up of the device, electrical flex-circuit contacts, and I/O fiber ferrule on the cylindrical metal header.

It is essential to minimize polarization dependent loss (PDL) in the system. We selected a grating with a blaze wavelength at 1.85μm wavelength with equal efficiencies (0.8dB loss) for S and P polarizations at 1.55μm. To eliminate small residual wavelength variance of the PDL, a zero order quarter wave plate is placed between the lens and the grating and orientated to rotate the polarization of the light by 90° upon two passes, such that the total efficiency for arbitrary input polarization light is the product of the S and P efficiency of the grating.

The photographs in Fig. 3 show the new opto-mechanical mounting, which consists of a 150 mm-long metal tube, a lens, a grating on a locking tip/tilt mount, and a cylindrical metal header. An 8 mm-square MEMS die is mounted on the 25 mm-diameter header. The 1.5 mm-long active MEMS etalon stripe is positioned next to an anti-reflection coated APC ferrule, which acts as both input and output from the package. Traces on the chip are wire bonded to two identical flexible circuits, which connect 40 pairs of active leads and two grounds to the drive electronics. The system was designed to maintain the focal plane at the MEMS mirror over a 60 degree Celsius temperature range. The lens and grating mounts, tube, and header are fabricated of super-invar metal. Tests indicated a spectral shift of around 0.001nm per degree C, or about 7.5GHz over 60 degrees. This optical system is appropriate for constructing systems operating from 1500 nm to 1630 nm.

There are just four alignments, all orthogonal: the device submount slides axially for focus, the grating is tip/tilt adjusted to position the selected center wavelength on the device, and rotated around the tube axis to align the dispersed spectra with the device window. The alignment process uses a broad spectrum amplified spontaneous emission (ASE) source and an optical spectrum analyzer. First, the lens and grating are inserted and locked in place (to an accuracy of 1 mm) then the device submount is inserted and focused to peak output power. Grating tip and tilt are used to center the desired spectrum on the device window, aided by alignment marks on the die. The grating rotation is fine-tuned to align the spectral dispersion with the MEMS device window. Then the focus, tip and tilt are fine-tuned before locking. In this prototype locking was done with screws; in a manufactured product, locking would be by laser welding. Alignment of the entire system requires about 5 minutes, compared with approximately four hours for the previous platform.

The optical performance of the system met initial design goals. The lens in an 8f configuration with mirror at the back focal plane has an insertion loss of 2.4dB at 1550nm, with a 0.2dB variation from 1500nm to 1620nm. The coupling losses are those from the aberration of the optical system and from the 40 anti-reflection coated surfaces and the residual glass absorption. Loss could be reduced with more stringent specifications, especially on lens coatings. The grating has 1.7dB loss on two passes with alternate polarizations, which could also be improved. This gives a 4.1 dB insertion loss for the optical system. Two passes through the circulator adds 1.3 dB, and the MEMS membrane 1.5 dB, to give an expected insertion loss of 6.9 dB. The assembled device had 7 dB loss, 0.2 ps/nm chromatic dispersion and less than 0.1ps polarization mode dispersion. The measured polarization dependent loss is less than 0.25 dB across the entire spectrum. The following experimental results were obtained using MEMS devices in this improved optomechanical package.

III. Linearized Voltage Response MEMS Device

The MARS (mechanical anti-reflection switch) micro-mechanical modulator was originally developed for digital data transmission, and later used as a high-speed analog variable attenuator. The basic structure is a quarter-wave dielectric antireflection coating suspended above a silicon substrate [15]. A silicon nitride layer with ¼λ optical thickness, separated from the silicon substrate by a fixed ¾λ spacer, acts as a dielectric mirror with about 70% (-1.5 dB) reflectivity. Voltage applied to electrodes on top of the membrane creates an electrostatic force and pulls the membrane closer to the substrate, while membrane tension provides a linear restoring force. When the membrane gap is reduced to λ/2, the layer becomes an anti-reflection coating with close to zero reflectivity. Like glass, the deformable nitride layer is brittle; the devices are defined as membranes because lateral stress is the dominant force. Mechanically, the device moves by elastic deformation, similar to a tuning fork. Electrically, the device behaves as a tiny capacitor, with zero static power dissipation regardless of reflectivity state.

MARS device fabrication begins with deposition of a spacer layer of phospho-silicate glass (PSG) equal in thickness to the desired air gap. Next, a film of silicon nitride, with thickness set to achieve an optical path delay of ¼ of the center operating wavelength, is deposited on the PSG layer. Both the PSG and silicon nitride films are deposited using conventional LPCVD techniques. Electrodes, comprising a thin layer of adhesion metal (such as titanium or chrome) and a 100 nm-thick layer of gold, are deposited using a lift-off procedure. Finally, reactive-ion-etching is used to open etch access holes through the silicon nitride film exposing the PSG film. The optical window is formed and made mechanically-active by a timed hydrofluoric acid etch and rinse.

Starting from the MARS modulator structure, a WDM equalizer can be fabricated by forming a stripe membrane lined on both sides of the optical window by mated pairs of individually-addressable electrodes, as illustrated in Figure 1. The WDM signal is then spectrally dispersed along the length of the optical window. The 0.24 μm vertical deflection required to move from maximum to minimum reflectivity is three orders of magnitude smaller than the 200 to 1500 μm width and length of the membrane, making them extremely robust for literally trillions of cycles. The mechanical resonance time of such devices ranges from 0.1 to 10 microseconds depending on the surface geometry and material parameters, particularly on membrane stress. The system response depends on drive electronics and overall packaged device capacitance.

Our initial prototype equalizer [2] used an 1150 nm thick spacer, approximately ¾ of the operating wavelength. The zero-voltage state is highly reflectivity (~1.5 dB loss), decreasing to low reflectivity (>20dB loss) with approximately 70 V applied to a single actuator. Figure 4(a) shows the theoretical voltage response of this device as a function of normalized bias voltage. The reflectivity depends on illuminating wavelength, so the figure plots 6 curves ranging from 1520 to 1620 nm (at 100 nm increments). Voltage response is highly nonlinear, with most of the reflectivity change occurring from 80-100% of applied voltage.

The ¾λ-gap configuration was used so that the unpowered state of the device would be reflective (low throughput loss). However, this concern is not relevant to an equalizer used in conjunction with an amplifier, because an unpowered amplifier will absorb and block incident signals. Therefore we can consider the alternative device shown in Figure 4(b), where the initial gap is set at one wavelength, such that the unpowered reflectivity is relatively low This λ-gap device balances the nonlinear optical response of the optical etalon against the nonlinear voltage response of the micromechanical actuation. The reflectivity with zero bias depends strongly on wavelength, but for all wavelengths the voltage response is more linear.

The device actuation voltage depends on initial gap and the membrane stress as determined by the temperature and composition of the deposited layers. Using a silicon-rich silicon nitride layer, residual tensile stress was reduced from roughly 600 MPa to less than 100 MPa. This reduced the actuation voltage of the new λ-gap device from 70 V to 42 V, despite the increased gap.

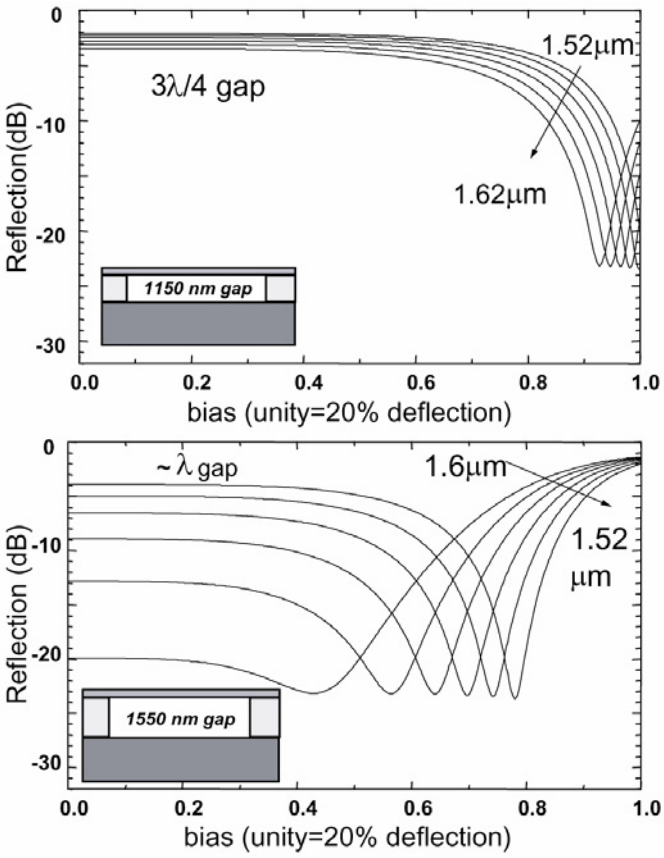

Figure 4: Micro-etalon reflectivity as a function of applied bias voltage for two initial air-gap spacings. Fig 4(a), the initial gap is 1150 nm, approximately ¾λ. In Fig 4(b) the initial gap is 1550 nm, approximately λ. In both cases the optical delay of the nitride membrane isλ/4.

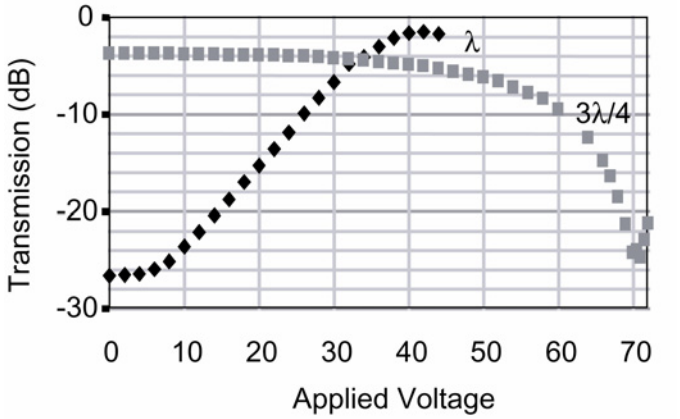

Figure 5: Reflection vs applied voltage for monochromatic illumination of a 3/4λ and improved λ device, showing greater linearity in response to a reduced drive voltage.

Figure 5 shows the voltage response of the initial ¾λ-gap device and of the low-stress λ-gap device measured at 1552 nm. At different wavelengths, the operating voltage range is shifted. The more gradual and nearly linear change in reflectivity of the λ device produces a more easily controlled response and is better suited to feedback stabilization using power monitoring.

Figures 6 and 7 show the full spectral response of the ¾λ- and λ-gap devices, respectively. Both can achieve high dynamic range (>25 dB) and are able to provide flat profiles, provided suitable drive voltage is applied. They also both show a 7 dB insertion loss over the 42 nm design spectra. Because the λ device has low unactuated reflectivity, it is necessary to apply a bias voltage during assembly to measure the insertion loss and achieve correct component alignment.

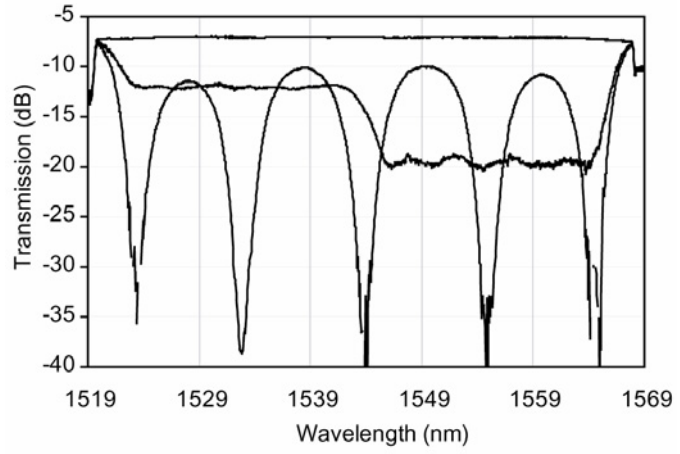

Figure 6: Spectral response of a 3/4λ device with several drive voltage settings. The top trace shows low and uniform insertion loss resulting from zero applied voltage. The trace with five deep features shows the output (and maximum dynamic range) when five single electrodes are actuated to maximum attenuation. The third trace shows the output when voltages are adjusted to achieve two uniform attenuation segments.

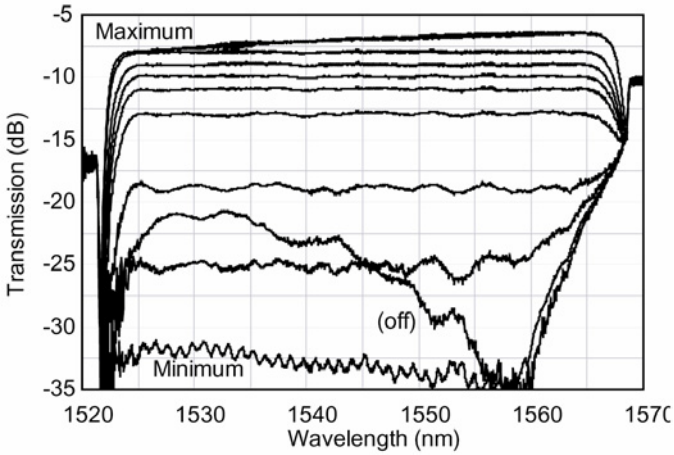

Figure 7: Spectral response of a λ-gap device. The trace labeled 'off' shows reflectivity with no applied voltage, while the trace labeled 'maximum' shows output with voltages across the array set to maximize output at each wavelength. The remaining traces show the output with voltages adjusted to obtain flat response from minimum (-32dB) to maximum (-7db) transmission.

IV. Extended C+L-band Equalizer

A flat-spectrum white light source was needed for testing of C+L-band components. It was possible to build this source using two separate 42 nm equalizers. However, since both the optomechanical package and MEMS device are capable of ultra broadband performance, a ¾λ membrane equalizer with 40 actuators spaced over a 4 mm length was fabricated and mounted in the same package. The insertion loss of the resulting 104 nm bandwidth spectral equalizer is shown in Figure 8. The minimum loss was less than 7 dB over the range of 1512 – 1600 nm, but increased to as high as 8 dB at 1618 nm. Fig. 8 also shows the attenuation created by 5 widely spaced features each adjusted for maximum attenuation to demonstrate that the equalizer is capable of greater than 15 dB attenuation over the full spectral range. Low source power limited the accuracy of measurements at the longer wavelengths, creating the noise seen in the difference spectra. The spectral features, at same attenuation levels, have the same width in the 105nm wide device as in the 42nm wide device (see following section) indicating that the feature size results from the mechanical membrane coupling and not the optical system resolution.

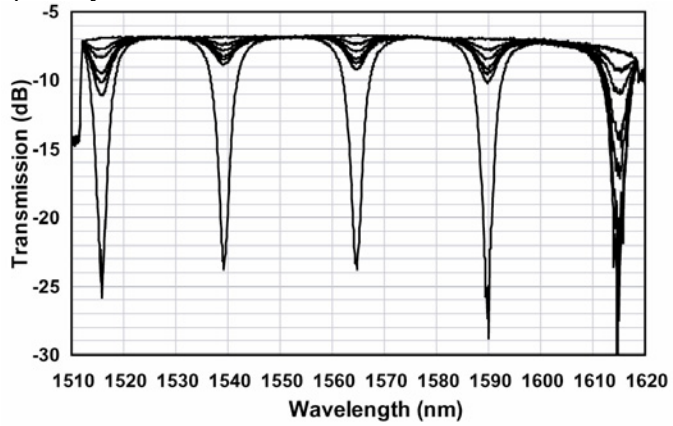

Fig. 8. Equalizer with 104 nm spectral bandwidth. Maximum drive voltage was <16V.

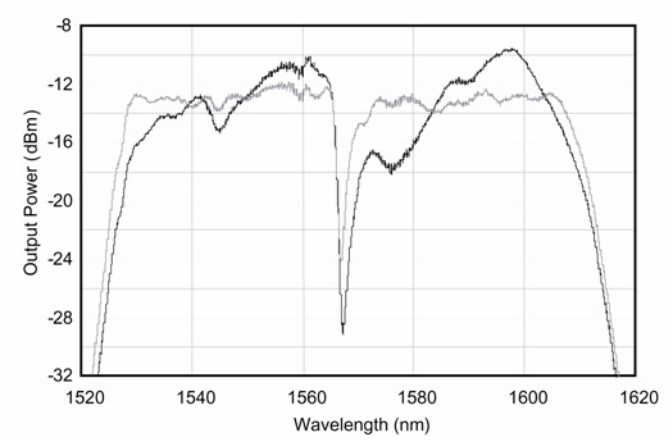

Fig. 9. Output from the same broadband spectral equalizer when used to flatten a broad spectrum (C- + L-band) ASE source. Traces before (black) and after equalization (grey) level-flattening are shown.

Figure 9 shows the resulting white light ASE source output before and after spectral equalization. Spectral uniformity across the 1528 nm – 1608 nm band was improved from 9 dB to +/-1 dB, aside from the deep valley between C and L bands.

The spectral width of the features could be reduced by using a longer MEMS device and a more dispersive grating system so the mechanical coupling would occur over a shorter spectral region. Compatible compact optical demultiplexing systems, with four to ten times larger spatial dispersions, have been demonstrated [10, 16] which would enable spectral resolutions of <1nm to be achieved. Longer devices also require lower actuation voltages; the device illustrated in Figure 8 required less than 16 volts for full attenuation.

V. Segmented "Ribbon" Channelized Equalizer

The spectral resolution of the equalizer with a 3/4λ device and a 1.5 mm-long strip membrane with 40 actuators is illustrated in Figure 10. One 10 dB-deep feature is created by applying voltage to a single actuator at 1528 nm (Channel #5), then each trace shows the inter-channel crosstalk as a second voltage is applied to successively closer actuators, each time adjusting both voltages to maintain a 10 dB depth on the center of both features. The continuous nitride membrane has a distance-dependent mechanical cross-coupling between all actuators. For the device tested, two individual 10 dB features create a >1 dB change from nominal maximum transmission midway between the features when separated by 9 nm, and >3dB when separated by 4.5nm. The features can only be considered distinct when separated by over 20nm. The equalizer thus imposes a smoothing function on any spectral profile created, regardless of feedback. This is preferable for gain flattening filters but useless for channelized filters, where, by definition, the attenuation on each channel is independent of its neighbors. For this application, it is necessary to physically decouple the adjacent channels of the etalon equalizer.

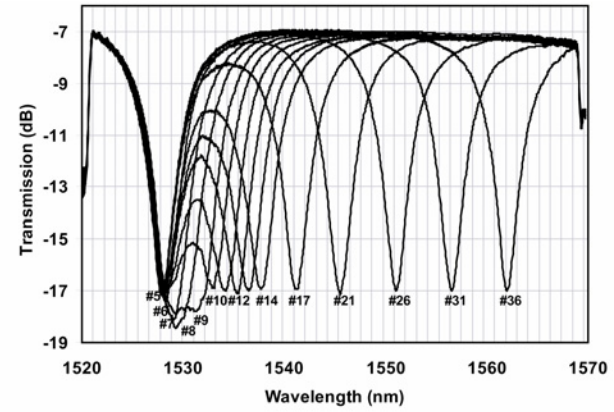

Figure 10: Spectral resolution of the continuous membrane DGEF, showing mechanical coupling between channels that prevent discontinuous spectral profiles.

In fact, the first conception of an etalon equalizer was based on providing one discrete equalizer device per spectral channel [2]. The equalizer stripe was composed of 32 adjacent bands, each 70 μm-long by 35 μm wide along the spectrally dispersed direction. This equalizer was only marginally functional, as the stress in each segmented equalizer element caused the bands to curl at the edges (like potato chips). The usable passband window was less than 10% of the 200 GHz channel spacing, making it unsuitable for practical systems. The solution for the DGEF was to use a continuous membrane, but another approach was needed for a channelized equalizer with fully independent attenuation at each wavelength data transmission channel.

One solution is to relieve the lateral stress in the membrane by slicing it into multiple thin ribbons with a common actuator. If the cuts between ribbons are smaller than the single-frequency spot size, then the cluster of ribbons still function as a variable-reflectivity etalon mirror. A representative device is shown in Figure 11. As for the DGEF, the device structure is a silicon rich silicon nitride λ/4 layer (n=1.9) suspended over the silicon substrate with an electrostatically controlled gap (initially 3λ/4). The individual actuators in this device were on a 36.75 μm pitch, but each actuator controls a sheet of Silicon Nitride cut with sub-micron-width gaps into 6 ribbons of 6um each. These slits were defined using e-beam lithography, and etched into the Nitride using reactive ion etching.

When voltage is applied to one of the gold-coated electrode pairs, force is applied uniformly to the set of six ribbons, causing them to deflect towards the substrate and reduce etalon reflectivity from high (-1.5dB) to low (–20dB). The packaged device achieves an insertion loss of 8dB.

The system produces a spectral spacing and hence system resolution of 1.1 nm for individual actuators, compared with the spectral resolution of 5 to 10 nm (depending on definition) for the DGEF. Figure 12 illustrates the response of a single actuator with 0 to 14V applied, producing 20 dB dynamic range. Figure 13 illustrates attenuation patterns created by actuating from one to seven different channels. The small ripples visible in the spectrum of Figure 13 are caused by the illuminating 10.5 μm $1/e^2$ mode field diameter sampling the ribbons and spaces.

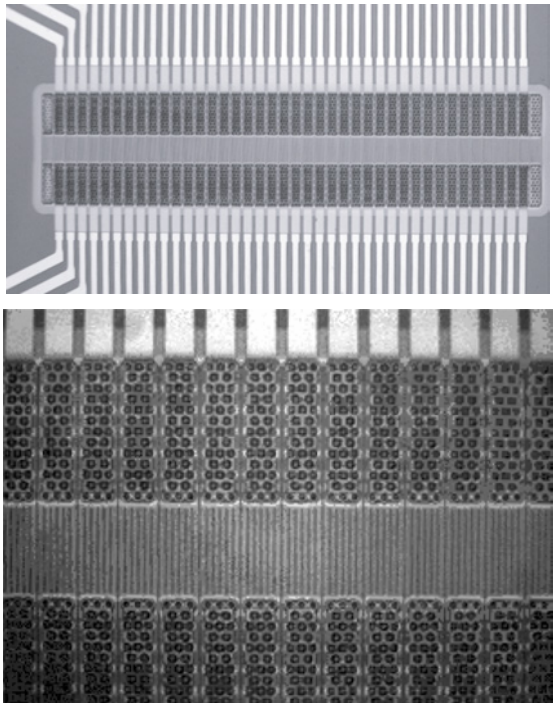

Figure 11: Segmented equalizer device with 40 discrete mechanical actuators controlling 240 segmented ribbons plus two sets of unactuated ribbons at the ends. Top, entire device, showing 1.5 mm optical window; below, closeup of segmented equalizers, showing individual ribbons.

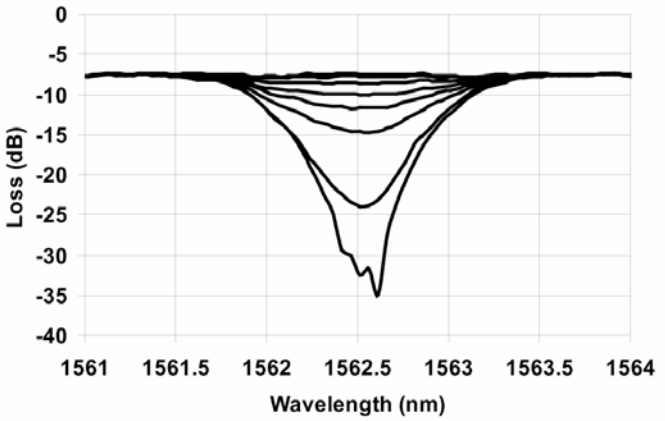

Figure 12: Spectrum of single channel actuation at 0V, 5V, 8V, 10V, 11V, 12V, 13V, 14V.

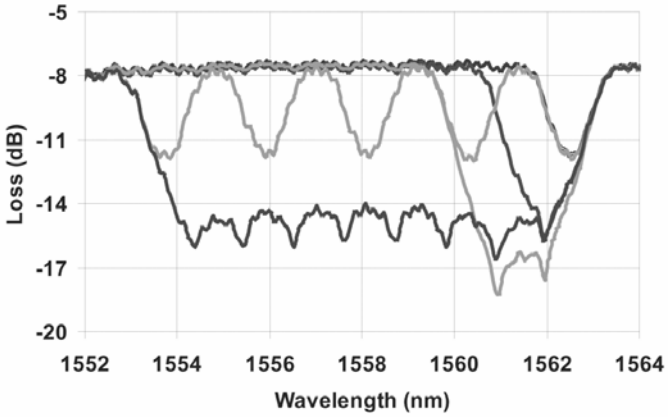

Figure 13: Various attenuation spectra achieved by actuating from one to seven channels.

These preliminary experimental results constitute a proof-of-principle for the segmented device; improving the uniformity across the passband would require further reduction of the spacing between ribbons. With physical segmentation of the actuators, creating a desired channel passband is achieved by selecting a suitable device pitch, limited only by the optical spot size illuminating the device.

VI. Self-Equalized Erbium Amplifier

Finally, we show how a straightforward use of the DGEF filter can dramatically enhance the operational versatility of a conventional erbium fiber amplifier. The amplifier chosen was a C-band EDFA originally used in the first MONET transmission system [17], designed to provide uniform gain for 16 input channels with -8 dBm per channel. Our goal was to increase the operating bandwidth from 12 nm to 30 nm, while at the same time increasing the allowable input power level range to 15 dB, all while maintaining less than 1 dB power non-uniformity. This capability could be used in upgrading the transmission capacity of an existing fiber span.

The original MONET amplifier provided access between two gain stages for dispersion-compensating fiber. Instead, a 42 nm-bandwidth DGEF filter was inserted between the two gain stages, as shown in Figure 14. A 1% output power tap was monitored by an optical spectrum analyzer connected to a PC. The PC controlled the DGEF using a simple iterative feedback stabilization algorithm incorporating a mathematical model of device voltage response.

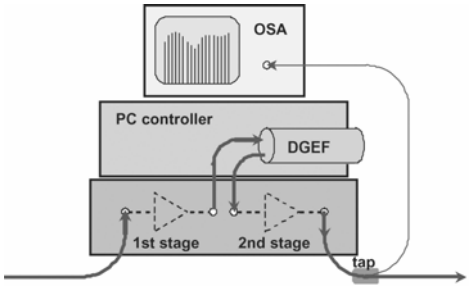

Fig. 14. Amplifier layout, with a computer-controlled dynamic gain equalization filter between two gain stages.

The amplifier was tested using 36 lasers distributed over a 30 nm optical band and set at approximately equal input powers (under 1dB level variation). The 36 signals passed through a common attenuator used to simulate loss from a variable fiber span length. The top row of traces shown in Figure 15 show the output spectra for decreasing average input power (increasing span length) with equalization turned "off" (set to uniform maximum internal transmission). The average input power levels are –13 dBm/channel (top left), –18 dBm/channel (top center) and –23 dBm/channel (top right). The respective output intensities vary by up to 7 dB, signifying poor amplifier configuration. Based on this performance for a single amplifier, the effect of cascading several such non-uniform amplifiers would be catastrophic.

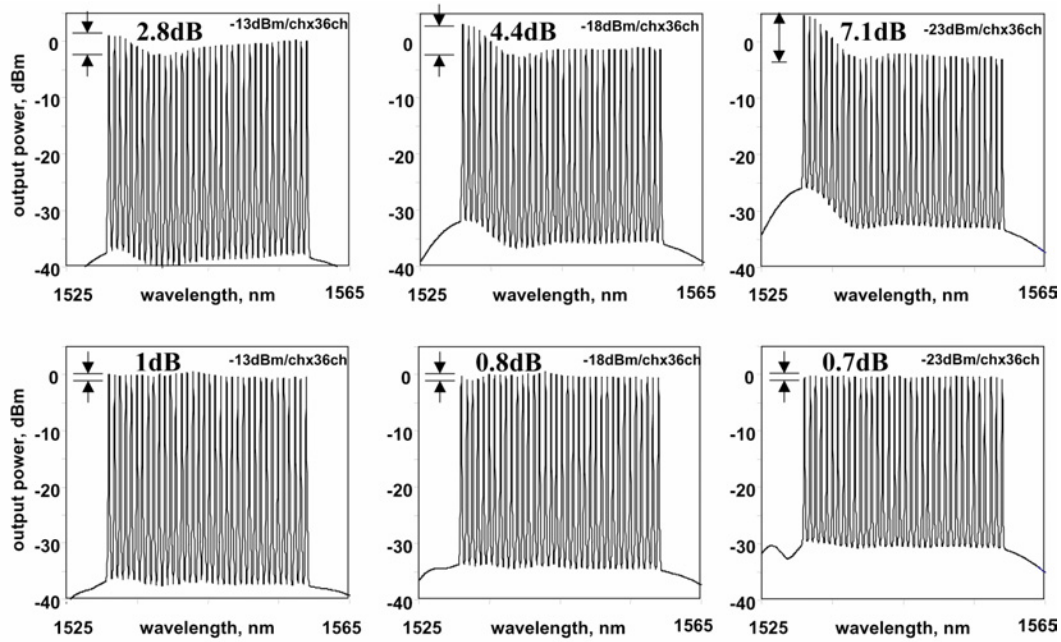

Figure 15: Amplifier output as input power drops by 5, 10 and 15 dB from nominal without (top row) and with (bottom row) active spectral equalization.

However, when the equalizer is turned "on" (using feedback to create compensating attenuation profiles) the outputs converge to 1 dB or lower variation for all cases, as seen in the bottom row of traces in Figure 15. In this case the feedback signal is local to the DGEF, but it is possible to remotely monitor the optical power levels and use this signal to control a single equalizer at mid-span, thereby providing end-to-end equalization. In practice, the number of equalizers needed would depend on the allowed mid-span power divergence before an unacceptable level of nonlinear transmission impairment occurred.

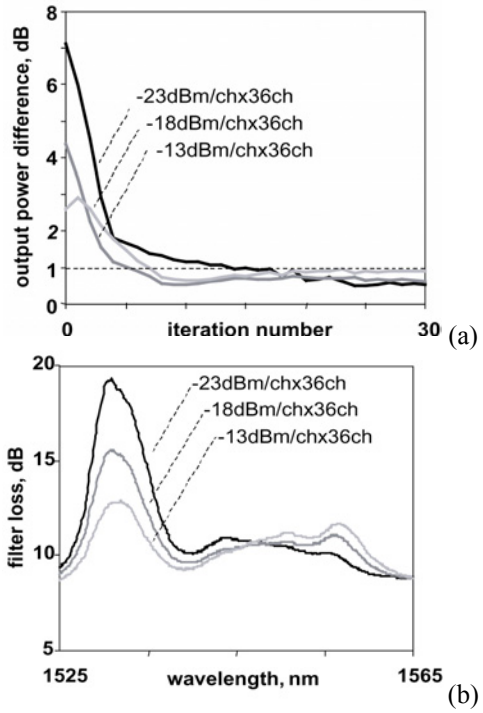

Figure 16: (a) Output power variation as a function of time after a sudden change in input power level, (b) the resulting gain equalization filter profiles.

Figure 16(a) shows output power convergence as a function of time following a sudden drop in input intensity. Each feedback loop iteration required about 0.5 seconds for the optical spectrum analyzer to collect and transfer the spectrum, but using a fast power monitor would reduce this to less than 100 ms.

Figure 16(b) shows the steady state attenuation profiles of the equalization filter, from which the compensation of the gain tilt is apparent. The filter has a uniform minimum insertion loss of about 7 dB, and applies an additional loss of up to 10 dB as the input power decreases. Because the amplifier is operated in a gain-saturated regime, the resulting output power is not significantly affected. The noise figure (indicated by the ASE level between signals) does show some increase, but maintains a signal to ASE difference of 30 dB or more.

VII. Conclusions

Dynamic channel equalization may be implemented with various device technologies, or even combined with other network functions such as channel monitors and transparent switching. Clearly, dynamic spectral filters can be constructed using free-space or waveguide demultiplexing in combination with a variety of actuator technologies. In this paper we have shown a range of equalizers based on micromechanical etalons, including device structures for reduced drive voltage, more linear response, and great spectral resolution. We have also demonstrated the utility of dynamic gain equalization filters for creating more versatile amplifiers and, by extension, WDM transmission systems. We believe that dynamic channel equalization, however it is implemented, is well on its way to becoming an essential function in WDM networks.

REFERENCES

[1] W. J. Tomlinson, 'Dynamic gain equalization for next-generation DWDM transport systems', Ultralong Haul DWDM Transmission and Networking / WDM Components, 2001 Digest of the LEOS Summer Topical Meetings, 30 July-1 Aug. 2001 p2.

[2] J. E. Ford, J. A. Walker, M. C. Nuss and D. A. B. Miller, "32 channel WDM graphic equalizer," Digest, *IEEE/LEOS Summer Topical Meeting on Broadband Optical Networks*, Keystone CO, 1996.

[3] J. E. Ford and J. A. Walker, 'Dynamic spectral power equalization using micro-opto-mechanics', IEEE Photonics Technology Letters, Vol. 10(10), pp. 1440 –1442, 1998.

[4] A. Ranalli, B. Scott, and J. Kondis, "Liquid Crystal – Based Wavelength Selectable Cross-Connect," European Conference on Optical Communications, Nice, France, pp. 68–69, 1999.

[5] J.K. Rhee, F. Garcia, A. Ellis, B. Hallock, T. Kennedy, T. Lackey, R.G. Lindquist, J.P. Kondis, B.A. Scott, J.M. Harris, D. Wolf, M. Dugan, 'Variable passband optical add-drop multiplexer using wavelength selective switch', European Conference on Optical Communication, ECOC '01. 27th, Volume: 4 , 2001 Page(s): 550 –551 2001.

[6] O. Bouevitch, D. Touahri, J. P. Morgan, S. Panteleev, C. Reimer, 'Channel-power equalizer and dynamic gain equalizer based on the optical bench platform' IEEE/LEOS Summer Topical Meetings on All-Optical Networking: Existing and Emerging Architecture and Applications/Dynamic Enablers of Next-Generation Optical Communications Systems/Fast Optical Processing in Optical Transmission/VCSEL and Microcavity Lasers. 2002, 15-17 July 2002 Page(s): MD1-4 -MD1-5 (2002)

[7] J.-C. Chiao 'Liquid-crystal optical harmonic equalizers' Advanced Semiconductor Lasers and Applications/Ultraviolet and Blue Lasers and Their Applications/Ultralong Haul DWDM Transmission and Networking/WDM Components, 2001 Digest of the LEOS Summer Topical Meetings , 30 July-1 Aug. 2001 pp. 39-40

[8] H. S. Kim; S. H. Yun; H. K. Kim; N. Park; B. Y. Kim, 'Dynamic gain equalization of erbium-doped fiber amplifier with all-fiber acousto-optic tunable filters' Optical Fiber Communication Conference and Exhibit, 1998. OFC '98., Technical Digest , 22-27 Feb. 1998 Page(s): 136 –138

[9] C.R. Doerr, C. H. Joyner, L. W. Stulz, "Integrated WDM dynamic power equalizer with potentially low insertion loss" IEEE Photonics Technology Letters, 10(10) pp. 1443-1445, Oct. 1998

[10] D.T.Neilson, D.S.Greywall, S.Chandrasekhar, L.L.Buhl, H.Tang, L.Ko, N.R.Basavanhally, F.Pardo, D.A.Ramsey, J.D.Weld, Y.L.Low, J.Prybyla, R.Scotti, A.Gasparyan, M.Haueis, S.Arney, S.P.O'Neill, C-S.Pai, D.H.Malkani, M.M.Meyers, N.Saluzzi, S.H.Oh, O.D.Lopez, G.R.Bogart, F.P.Klemens, M.Luo, J.Q.Liu, K.Teffeau, A.Ramirez, K.S.Werder, J.E.Griffith, C.Frye, M.V.Kunnavakkam, S.T.Stanton, J.A.Liddle, H.T.Soh, T-C.Lee, O.Nalamasu, K.C.Nguyen, 'High-dynamic Range Channelized MEMS Equalizing Filter', Optical Fiber Communication Conference and Exhibit 2002, OFC 2002, pp586-588 (2002).

[11] D. M. Marom, D. T. Neilson, D. S. Greywall, V. Aksyuk, M. E. Simon, N. R. Basavanhally, P. R. Kolodner, Y. L. Low , F. Pardo, C. A. Bolle, C. S. Pai, D. López, J. A. Taylor, J. E. Bower, J. Leuthold, M. Gibbons, and C. R. Giles 'Wavelength selective 4×1 switch with high spectral efficiency, 10 dB dynamic equalization range and internal blocking capability' ECOC 2003 September 21-25, 2003, Rimini, Italy, Paper Mo3.5.3 (2003).Giles 'Wavelength selective 1×4 switch for 128 WDM channels at 50 GHz spacing," Optical Fiber Communications Conference and Exhibit 2002, OFC 2002, pp. 857-859 (2002).

[12] C. R. Doerr, L. W. Stulz, R. Pafchek, S. Shunk, 'Compact and low-loss manner of waveguide grating router passband flattening and demonstration in a 64-channel blocker/multiplexer', IEEE Photonics Technology Letters, 14(1), pp. 56-58, Jan. 2002.

[13] J. E. Ford, J. A. Walker, K. Goossen and D. T. Neilson, 'Broad spectrum micromechanical equalizer,' European Conference on Optical Communications 1999, Nice, France Sept. 26 (1999).

[14] J. E. Ford, "Optomechanical platform" U.S. Patent 6,307,657; October 23, 2001.

[15] J. E. Ford, J. A. Walker, D. S. Greywall and K. W. Goossen, "Micromechanical fiber-optic attenuator with 3 microsecond response,**"** *IEEE Journal of Lightwave Technology* **16**(9), 1663-1670, September 1998.

[16] D. T. Neilson, R. Ryf, F. Pardo, V. A. Aksyuk, M-. E. Simon, D. O. Lopez, D. M. Marom, S. Chandrasekhar, 'MEMS based Channelized Dispersion Compensator with Flat pass bands using an arrayPassbands," IEEE Journal of deformable MEMS mirrors' Optical Fiber Communication Conference, 2003, PD 29 (2003)Lightwave Technology, Vol. 22, No. 1, pp. 101-105 (2004).

[17] W. T. Anderson, J. Jackel, G.-K. Chang, H. Dai, W. Xin, M. Goodman, C. Allyn, M. Alvarez, O. Clarke, A. Gottlieb, F. Kleytman, J. Morreale, V. Nichols, A. Tzathas, R. Vora, L. Mercer, H. Dardy, E. Renaud, L. Williard, J. Perreault, R. McFarland, and T. Gibbons "The MONET project - a final report." *IEEE Journal of Lightwave Technology* 18(12) pp. 1988 -2009, Dec. 2000.

Joseph E. Ford received a B.Sc. degree in physics from UCLA in 1983, and Masters degrees in laser physics and optical engineering from the University of British Columbia and Rochesters Institute of Optics, respectively. In 1992 he received his Ph.D. degree in electrical engineering/applied physics from the University of California, San Diego (UCSD). From 1994 to 2000, in the Advanced Photonics Research Department of Lucent Bell Laboratories, Holmdel, NJ, he worked on integrating surface-normal optoelectronic and micromechanical devices with single-mode fiber for optical modulation, switching, and data transmission. From 2000 to 2002 Dr. Ford was at Optical Micro-Machines, an optical switching startup. In 2002 Dr. Ford became as Associate Professor in UCSDs Department of Electrical and Computer Engineering, where he started the Photonics Systems Integration Laboratory.

David T. Neilson (M'96-SM'02) received the B.Sc.(Hons) degree in physics from Heriot-Watt University in 1990 and the Ph.D. degree in physics for work on optical nonlinearities in InGaAs Quantum well devices from Heriot-Watt University in 1993.
He was a post doctoral researcher at Heriot-Watt University from 1993 to 1996 working systems and devices for free space optical interconnects. From 1996 to 1998 he was a Visiting Scientist at NEC Research Institute, Princeton, NJ researching optical interconnects for high performance computing. In 1998 he joined Bell Labs where he has worked on MEMS based crossconnects, wavelength selective switches, equalizers and dispersion compensators. He is currently a technical manager with responsibility for optoelectronic device growth and fabrication facility. He has over 80 publications in the field of optical interconnects and switching.
Dr Neilson is a senior member of the IEEE, LEOS and a member of the OSA.

Seo Yeon Park received the B.S. and M.S. degrees in electonics engineering from Yonsei University, Seoul, Korea, in 1987 and 1989, respectively, and Ph. D. in electrical engineering from Korea Advanced Institute of Science and Technology, Taejon, Korea, in 1998.
Between 1989 and 1998 he was with Elctronics and Telecommunications Research Institute, Taejon, Korea, as a research engineer. From 1999 to 2000 he was a member of technical staff at Bell Laboratories, Advanced Optical Networking Center, Lucent Technologies. From 2000 to 2002 he was with Sycamore Networks as a principal system engineer. In 2003 he joined Optovia Corporation, Acton, MA, as an optics design lead. His interests include optical amplifiers, optical fiber communications, and WDM optical networkings.